SOTECH Vol. 11, No. 4, pp. 29 ~ 54, 2007

# Sensitivity Study of Smoothed Particle Hydrodynamics

Yooil Kim[1], Bo-Woo Nam[1] and Yonghwan Kim[1]

[1] Department of Naval Architecture and Ocean Engineering, Seoul National University, Seoul, Korea;
Corresponding Author: yhwankim@snu.ac.kr

**Abstract**

Systematic sensitivity analysis of smoothed particle hydrodynamics method (SPH), a gridless Lagrangian particle method, was carried out in this study. Unlike traditional grid-based numerical schemes, systematic sensitivity study for computational parameters is very limited for SPH. In this study, the effect of computational parameters in SPH simulation is explored through two-dimensional dam-breaking and sloshing problem. The parameters to be considered are the speed of sound, the type of kernel function, the frequency of density re-initialization, particle number, smoothing length and pressure extraction method. Through a series of numerical test, detailed information was obtained about how SPH solution can be more stabilized and improved by adjusting computational parameters.

**Keywords: smoothed particle hydrodynamic method (SPH), sensitivity analysis, parametric study**

## 1 Introduction

Since its first application to astrophysics problems in 1977 by Lucy, Gingold and Monaghan, the smoothed particle hydrodynamics method (SPH) steadily has been extended its field to various physical problems from large-deformation solid mechanics to compressible/incompressible fluid dynamics. Lucy et al. created a method based on the concept of particle-in-cell (PIC), where convection is handled by particles in cell whereas pressure field by finite difference scheme. What makes SPH different from PIC is that pressure in SPH is estimated by interpolating a state variable defined at each particle. Particles are accelerated or decelerated by pressure gradients which are obtained by differentiating so called smoothing function or kernel function. Each moving particle carries this kernel function with it, and whole computational domain is interpolated by summing up the physical quantity of neighboring particles with proper weighting factors.

There are many benefits that can be obtained by using SPH in hydrodynamic problems, especially when violent free surface is of primary concern. Since SPH is pure Lagrangian approach, there is no need for additional treatment for free surface reconstruction. Unlike Eulerian methods that free-surface capturing work is relatively difficult, working in Lagrangian frame is naturally suited for capturing evolution of free boundary or surface without any additional cost. In some aspects, SPH resembles finite element method (FEM)

in that both numerical methods require a proper interpolation of state variable to handle continuum media. Domain interpolation in FEM is based on the node along with its connectivity definition which is called element. However, domain interpolation in SPH does not require connectivity information since interpolation is made based on the particles inside certain sub-domain, i.e. compact support. This leads to the advantages of SPH over FEM that particle can freely move in Lagrangian way without the termination of analysis, though there are some loss of interpolation accuracy, e.g. the loss of partition of unity property. Unlike grid methods, SPH does not produce any large algebraic equation in solving the governing equation. Because the motion of fluid is represented by the motion of corresponding particle, momentum conservation equation is directly applied to each particle. The only thing that needs to be considered is how particles are interacting with each other, which is realized by smoothing process.

Monaghan and Kos[1] contributed a lot to the extension of SPH application from traditional astrophysics to incompressible fluid problems, such as propagation of gravity wave. Libersky and Petschek[2] extended SPH to solid media where full 3D stress tensor and strength of material need to be considered. The introduction of material strength into SPH highlighted some fundamental shortcomings of the method such as particle inconsistency, tensile instability and zero energy mode. By relating the tensile stress with the first derivative of kernel function, Swegel, Hicks and Attaway[3] gave a detail description in their paper why SPH inherently suffers from instability problem. As a remedy for this tensile instability, Monaghan[4] proposed the use of artificial pressure term in momentum equation which prevents particle clumping caused by the instability. Dilts[5,6] derived Lagrangian SPH discrete equation by applying Galerkin procedure to the Eulerian conservation laws and developed consistent meshless algorithm. Aforementioned tensile instability is actually the motivation of Dilts' work. Later on, researchers tend to focus more on the accuracy and consistency of the interpolation itself leading to works on reproducing kernel particle method (RKPM) or moving least quare method (MLS), which later become popular meshless method. The original SPH method tends to be poor when particles are not uniformly distributed, giving birth to the variety of modification or correction to the original kernel approximation. RKPM and MLS are two major streams of such enhancement though two are quite close to each other in terms of their basic ideas and final forms. In this sense, SPH can be said to be the early form of the meshless methods.

In this paper, systematic parametric studies have been carried out to figure out how each analysis parameter alters SPH simulation and its results. Some of them are relevant to the effectiveness of simulation, some others to the accuracy improvement of SPH, and others are to the convergence of the analysis results.

A two-dimensional dam-breaking problem was chosen as a sample problem for sensitivity study. Dam-breaking problem contains variety of fluid motion from stable collapse of fluid body to extremely violent free surface flow, not to speak of splash formation and wave breaking phenomenon. The influence of the number of particles used in the analysis was examined. The effect the number of particle has on the analysis result must be one of the most intriguing items among others, as the effect of spatial resolution, i.e. mesh size, in grid based method is the case. Since most SPH simulation is based on the weakly compressible approach, where actually incompressible fluid is assumed to be weakly compressible one, the speed of the sound is very important analysis parameter. It also has a lot of things to do with the determination of stable time increment size as well as particle spattering phenomenon in SPH simulation. The speed of sound was discussed in depth through numerical test and the analysis on the momentum conservation equation.

Periodic density reinitialization technique was originally proposed by Colagrossi[7], which improves pressure field by filtering out spikiness induced by weakly compressible assumption. Frequency of this density reinitialization is quite influential to the smoothness of pressure field and pressure time history. It was examined in detail how SPH simulation results improve as the frequency of density reinitialization increases. Finally, the type of the smoothing function and smoothing length was discussed. Historically, the type of smoothing fucntion used in kernel approximation has been one of the hottest topic because smoothing funciton itself is directly related to the accuracy of interpolation and also stability issue of SPH simulation. Dam breaking problem was analyzed with different type of smoothing fucntion and discussion was made on the characteristics of each smoothing function.

## 2 Basic formulation

Whatever the numerical scheme of interest is, what should be done first is to determine how to discretize or interpolate the whole computational domain. In SPH, a computational domain is discretized by a number of particles which can freely move without any connectivity among each other. Figure 1 tries to illustrate the commons and differences between finite element (FE) interpolation and meshless interpolation.

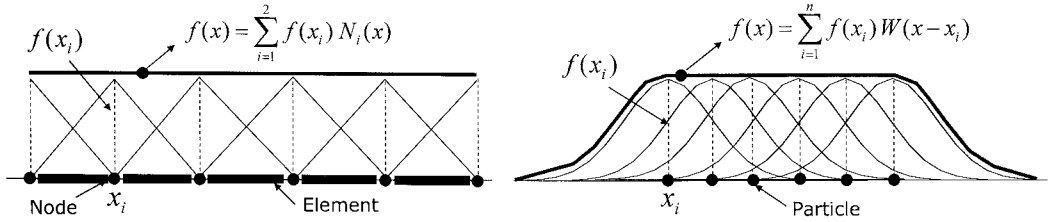


(a) Finite element interpolation (b) Meshless interpolation

**Figure 1:** Linear FE interpolation vs. Meshless interpolation

In the FE interpolation, as shown in Figure 1(a), constant field can be reproduced exactly by summing up the shape function which is defined inside each element. Even if node separates from each other due to the motion of underlying material, the way of interpolation wouldn't change since shape function itself expands and shrinks as element deforms. In case of meshless interpolation, each particle carries pre-defined kernel function (bell-shaped, in general), and constant field is reproduced by summing up all relevant kernel function. Major difference between the two is that meshless interpolation is global interpolation, which means that any relevant kernel function inside computational domain participates in the interpolation process, while the FE approximation is done locally, i.e. only shape function inside relevant element is used for the interpolation. It is obvious that the meshless method is far better than FEM when a continuous media is handled with large deformation in Lagrangian way, because mesh distorsion problem will never stop the simulation.

$$f(\vec{r}) = \int_{\Omega} f(\vec{r}')\,W(\vec{r}-\vec{r}', h)\,d\vec{r}' \tag{1}$$

Eq. (1) shows how this meshless interpolation is carried out in integral sense. This equation can be interpreted as the summation of function, $f(\vec{r}')$, with weighting factor, $W(\vec{r}-\vec{r}',h)$, which depends on the kernel function and the distance between $\vec{r}$ and $\vec{r}'$. In a discrete form for a fluid particle with mass $m_j$ and density $\rho_j$, it can be written to

$$f(\vec{r}_i) \approx \sum_{j=1}^{N} f(\vec{r}_j) W(\vec{r}_i - \vec{r}_j, h) \frac{m_j}{\rho_j} \tag{2}$$

As mentioned above, this is the weighted average of function variables of surrounding particles. Summation is made over the particles which are inside influencing radius, *h*, often called support domain, as shown in Figure 2(a).

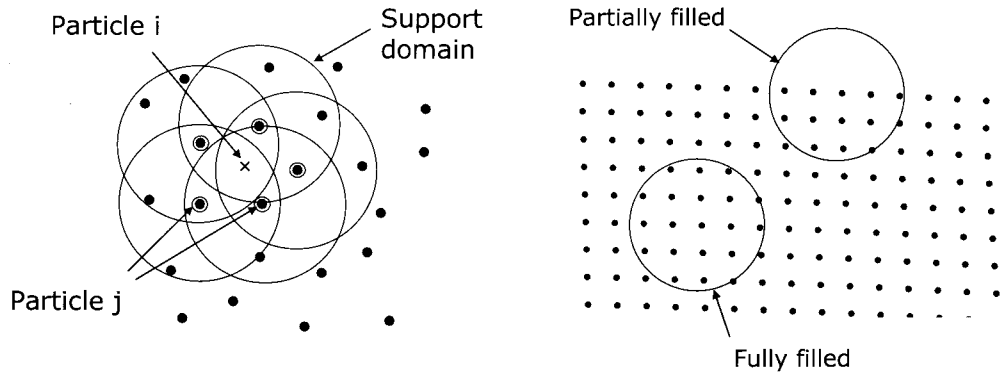


(a) Particle interaction (b) Particle deficiency

**Figure 2:** Particle interaction and deficiency

In some special cases, like particles located near the boundary of computational domain, the situation may arise that the number of surrounding particles is not sufficient enough causing particle deficiency problem, as shown in Figure 2(b). When this particle deficiency problem is met, kernel approximation needs to be normalized by dividing Eq.(2) by summation of weighting factor, as shown in Eq.(3). This is so called Shepard interpolation(Shepard[8]). The Shepard interpolation guarantees the reproducibility of constant field at most. If a field of the higher-order function is requested to be reproduced, other correction or modification needs to be done such as RKPM or MLS, which definitely increases computational cost.

$$f(\vec{r}_i) \approx \frac{\sum_{j=1}^{N} f(\vec{r}_j) W(\vec{r}_i - \vec{r}_j, h) \frac{m_j}{\rho_j}}{\sum_{j} \frac{m_j}{\rho_j} W(\vec{r}_i - \vec{r}_j, h)} \tag{3}$$

In most mechanical problems, governing equation requires the derivative of its state variable. Unlike FEM, where a weak form formulation is used for the approximation of only variable itself, SPH solves a strong form which the approximation of function

derivative is required as well. The function derivative can be easily calculated in SPH from the derivative of kernel function as,

$$\nabla f(\vec{r}_i) \approx -\sum_{j=1}^{N} f(\vec{r}_j) \nabla_i W(\vec{r}_i - \vec{r}_j, h) \frac{m_j}{\rho_j} \tag{4}$$

Once the domain interpolation is established, the governing equation(s) should be set up based on the discretized system. In the present study, the continuity and Euler equations, Eq. (5) and (6), are to be focused.

$$\frac{d\rho}{dt} = -\rho \nabla \cdot \vec{v} \tag{5}$$

$$\frac{d\vec{v}}{dt} = -\frac{1}{\rho} \nabla p + \vec{f} \tag{6}$$

In SPH, it is common approach to treat the fluid as weakly compressible one even though it is almost incompressible. This approach was firstly tried by Monaghan[9] in SPH framework ending up with fairly good results provided that Mach number inside fluid domain is small enough, generally less than 0.1. To keep this condition valid throughout analysis, the speed of sound in fluid's equation of state should be roughly 10 times of the expected maximum flow velocity. This weakly compressible approach does not allow us to force the time rate of fluid density in Eq. (5) to be zero. Eq. (5) and (6) can be transformed into discrete forms as follows:

$$\frac{d\rho_i}{dt} = \sum_j m_j \left( \vec{v}_i - \vec{v}_j \right) \cdot \nabla_i W_{ij} \tag{7}$$

$$\frac{d\vec{v}_i}{dt} = -\sum_j m_j \left( \frac{p_i}{\rho_i^2} + \frac{p_j}{\rho_j^2} + \Pi_{ij} \right) \nabla_i W_{ij} + \vec{f}_i \tag{8}$$

Eq. (7) and (8) can be easily obtained by using interpolation formula of function derivative as show in Eq. (4) along with some other mathematical procedures. $\Pi_{ij}$ in Eq. (8) is artificial viscosity introduced for numerical reason. When fluid is compressible, it is inevitable to have shocks inside the fluid domain, particularly around the region which pressure field varies so drastically that it behaves like discontinuous flow. Numerical problems caused by this shocks can be avoided by introducing the artificial viscosity in momentum equation, resulting in smooth pressure field around shock. Monaghan[10] proposed a modified artificial viscosity by combining both linear and quadratic term like,

$$\Pi_{ij} = \begin{cases} \dfrac{-\alpha_\Pi \bar{c}_{ij} \phi_{ij} + \beta_\Pi \phi_{ij}^2}{\bar{\rho}_{ij}} & \vec{v}_{ij} \cdot \vec{x}_{ij} < 0 \\ 0 & \vec{v}_{ij} \cdot \vec{x}_{ij} \geq 0 \end{cases} \tag{9}$$

where

$$\phi_{ij} = \frac{h_{ij}\vec{v}_{ij}\cdot\vec{x}_{ij}}{|x_{ij}|^2+\varphi^2},\ \bar{c}_{ij} = \frac{c_i + c_j}{2},\ \bar{\rho}_{ij} = \frac{\rho_i+\rho_j}{2},\ h_{ij} = \frac{h_i+h_j}{2},\ \vec{v}_{ij} = \vec{v}_i - \vec{v}_j,\ \vec{x}_{ij} = \vec{x}_i - \vec{x}_j$$

$\alpha_\Pi$ and $\beta_\Pi$ are constants that determines the contribution of linear and quadratic terms to total dissipation. Throughout this study, only the linear artificial viscosity is considered where $\alpha_\Pi$ is set to be 0.03. c and ρ mean the speed of sound and the fluid density, respectively.

Eq. (10) is the state equation used broadly for many fluids. c is the speed of sound, $\gamma$ is a polytrophic constant which is normally set to be 7. As mentioned above, this weakly compressible approach is more beneficial than truly incompressible approach in that computationally expensive pressure-Poisson equation does not need to be solved. However, it is well known that weakly compressible approach is responsible for the spiky pressure field induced by extremely stiff equation of state.

$$p = B\left(\left[\frac{\rho}{\rho_o}\right]^\gamma - 1\right),\ B = \frac{\rho_0 c^2}{\gamma} \tag{10}$$

In SPH, imposing the wall boundary condition to moving particle is not simple work at all. Most popular scheme is the ghost particle approach which imaginary ghost particles are distributed outside the wall. The velocity and pressure of the ghost particles are mirrored from interior particles.

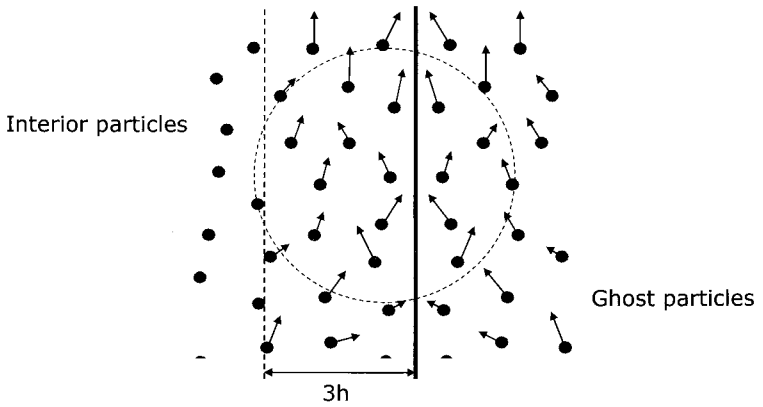


**Figure 3:** Ghost particle approach

Figure 3 shows how ghost particles are created and influence the motion of interior particles. Position, velocity and pressure of the interior particles located within three times of the size of compact support from the wall are mirrored outward to ghost particles. The mirrored ghost particles participate in the summation process of each interior particle whereas ghost particle itself does not evolve in time.

As shown in Eq. (7) and (8), SPH simulation is all about time marching of two state variables, density and velocity, meaning that the spatial derivative of smoothing function is

directly involved. Figure 4 explains why instability problem occurs in SPH simulation by relating particle position to the first derivative of smoothing function.

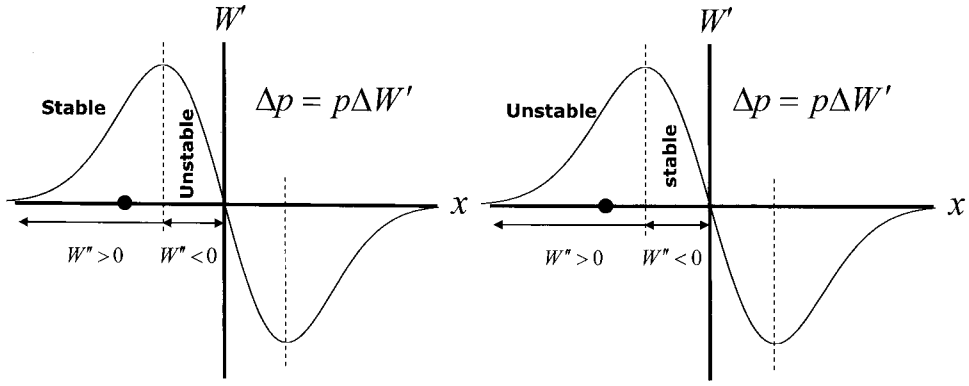


(a) Under compression (b) Under tension

**Figure 4:** Instability of SPH

When fluid is under compression, which is the case of Figure 4(a), particles stay stable while it is outside of dotted line, because, under this circumstance, pressure tends to increase as particle approaches to neighboring one. However, once it comes into the region inside of dotted line, it becomes unstable since pressure tends to decrease though particles get closer with each other. This is so called compressible softening. On the other hand, when fluid is under tension, situation becomes reversed. When particle is outside dotted line, pressure tends to decrease as particles get closer, which means system is unstable. However, once it gets inside dotted line it becomes stable. This is tensile instability problem. Since particles are initially placed with the distance of $h$, smoothing length, it can be easily understood that tensile instability is the primary concern, while the compressive softening is generally not. This was systematically analyzed by Swegel et.al.[3] with the details of stability analysis. Monaghan[4] proposed the use of artificial repulsive force to overcome tensile instability problem.

$$\frac{d\vec{v}_i}{dt} = -\sum_j m_j \left( \frac{p_i}{\rho_i^2} + \frac{p_j}{\rho_j^2} + \Pi_{ij} + R f_{ij}^n \right) \nabla_i W_{ij} + \vec{f}_i \tag{11}$$

Artificial pressure $f_{ij}$ becomes active only if either of interacting particles undergoes tensile pressure. When both are positive, extremely small artificial pressure becomes active to avoid local linear structure. This artificial pressure term was used in this study to avoid tensile instability problem.

Finding neighbor particles for SPH summation is one of the most time consuming tasks in SPH simulation. To minimize computational cost for this work, both linked-list search and pairwise interaction algorithm were used in this study. In the linked-list algorithm, whole computational domain is divided into many sub-cells, and particles are assigned to the cells, later being searched only for relevant cell. The pairwise interaction algorithm is removing extra floating point calculation by taking advantage of symmetry of governing equation.

## 3 Validation

Before directly jumping to the sensitivity analysis, validation work has been done for the developed code. 2 dimensional dambreaking and sloshing problem were chosen as sample problems and comparison was made between analysis results and measured experimental data. Figure 5 shows the detail dimension of 2D dam-breaking and sloshing problem. In case of dam breaking problem, the fluid was initially set to form a rectangle which is 0.6m high and 1.2m wide. The tank width is 3.22m. This dimensional feature is same as the experiment by Zhou et.al.[11]. For sloshing problem, test model in Figure 5(b) was chosen, which is identical to the test model studied by Van Daalen et.al.[12]. Varieties of filling ratio and excitation frequency were used for the numerical analysis.

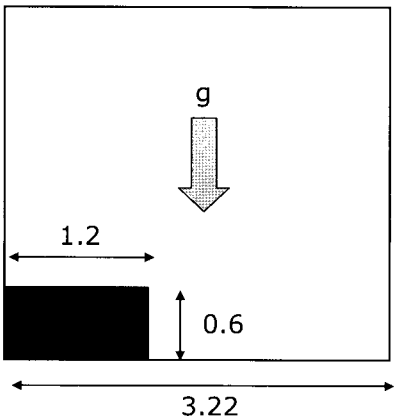


(a) Dam breaking problem

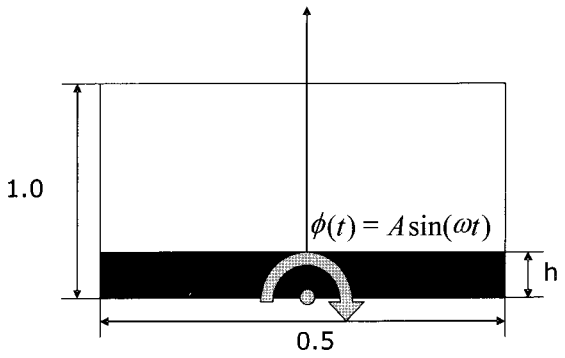


(b) Sloshing problem

**Figure 5:** Sample problems (unit: meter)

An effort was made for the validation of developed numerical code through the comparison with experimental data as well as numerical calculations done by others. Table 1 summarizes time evolution of the height and the surging front of collapsing dam.

**Table 1:** Evolution of dam height and surging front

| Time | Dam height | | | | Surging front | | | |
|---|---|---|---|---|---|---|---|---|
| | Exp.* | Monaghan | Liu | Present | Exp.* | Monaghan | Liu | Present |
| 0.71 | 0.90 | 0.90 | 0.90 | 0.90 | 1.33 | 1.56 | 1.45 | 1.55 |
| 1.39 | 0.76 | 0.75 | 0.75 | 0.75 | 2.25 | 2.50 | 2.38 | 2.50 |
| 2.10 | 0.57 | 0.56 | 0.56 | 0.57 | 3.22 | 3.75 | 3.50 | 3.72 |

(* by Monaghan[9], Locations normalized by its initial value, Time normalized by $\sqrt{HT_o/g}$ where $HT_o$ means initial dam height)

It can be seen that analysis results from this study is in good agreement not only with experimental result but also other SPH simulation results by Monaghan[9] and Liu[12].

Figure 6 shows SPH simulation results overlapped on experimental results(Zhou et.al.[11]) along with other analysis results(Colagrossi[7]). Wave height evolution from current study fits experimental data pretty well before overturning wave touches free surface back again, the moment when nondimensionalized time reaches 6.0. Wave height was measured at the location 2.7m away from the left vertical wall. Even after violent free surface becomes dominant in the flow, general trend is not so far from the experimental data. Other analysis results shown in Figure 6 are that of two phase SPH, two phase FVM with level set and BEM result. Gap between present study and others can be ascribed to the effect of air, whose influence to fluid flow becomes larger as violent free surface flow gets dominant.

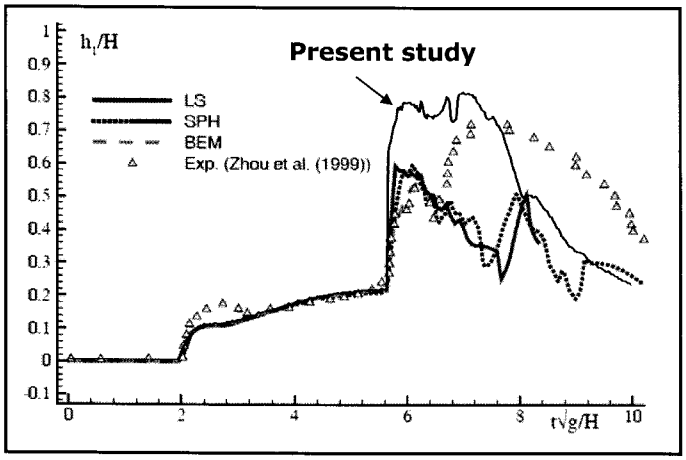


**Figure 6:** Comparison with experimental and computational results (Zhou et al. 1999, Present study with 11,250 particles)

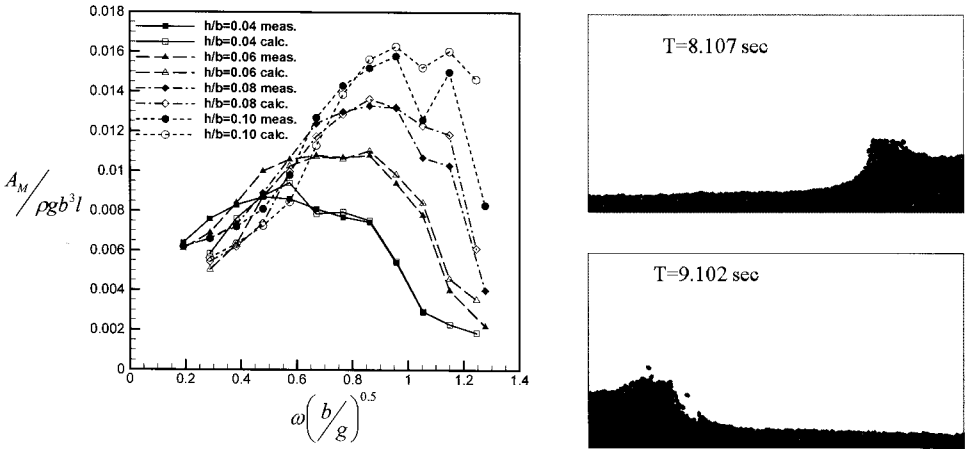


(a) Roll moment (b) Free surface

**Figure 7:** Global roll moement & free surface profile

2D sloshing problem was chosen as another validation sample problem. Figure 5(b) shows experimental setup for capturing global forces induced by violent fluid flow inside the tank. Tank was excited in harmonic way, whose motion center is located at the bottom of the tank. Roll moement, obtained from experiment was compared with SPH simulation results as shown in Figure 7(b). Comparison was made by exploring different filling ratio and excitation frequency. Correspondence between numerical simulation results and experiment is fairly good. Discrenpancy tends to increase as both filling ratio and excitation frequency become large, which is the case of the points at upper right corner of the Figure 7(a).

# 4 Sensitivity analysis

In the present study, the sensitivity of computational results was widely investigated through two-dimensional dam-breaking problem and sloshing problem which are covered in the previous section. A parametric study was done for following items

- Number of particle
- Speed of sound
- Frequency of density re-initialization
- Type of smoothing function
- Smoothing length
- Wall pressure (Pressure extraction method)

## 4.1 Number of particles

Firstly, the evolution of free surface was checked for the number of particles used in the analysis. The number of particle in SPH simulation may be comparable with the number of grids in grid-based method. Figure 8 shows the change of free surface profile when the number of particle is varied from 800, 1,800, 5,000 up to 20,000. Contour represents pressure field. It is clear that, as the number of particles increases, overall free surface profile tends to converge to a certain shape. Little difference can be found between the results of 5,000 and 20,000.

Figure 9 shows the variation of energy for the number of particles used in the analysis. Even though SPH simulation is that of compressible fluid, targeting physical phenomenon is the motion of incompressible fluid. This can be approximately achieved by the use of very stiff equation of state. Eq. (12) shows total energy decomposition into kinetic, potential, internal and dissipation energy. Energy change in Figure 8 considers only kinetic and potential energy among them because fluid flow in this analysis is assumed to be inviscid and incompressible. However, it should be noticed that, due to the compressibility and assumption and artificial viscosity, there is apparent loss of internal and viscous energy.

$$\begin{aligned} E_{TOT} &= E_{Kinetic} + E_{Potential} + E_{Internal} + E_{Viscous} \\ &= \int \frac{1}{2} \rho |\vec{v}|^2 dV + \int \rho g y dV + \int \rho e dV + E_{viscous} \end{aligned} \tag{12}$$

As shown in Figure 9(b), the energy loss to internal and viscous dissipation energy tends to decrease as the number of particle increases. Figure 9(a) shows that there are two distinctive points where energy loss changes its rate drastically. The first one happens around 0.5-sec when the surge front of collapsing dam hits right vertical wall. The second one happens around 1.5-sec when the front of overturning wave hits free surface backward. Both are the very moments that impact phenomena happen and the significant change of volume is induced in local impact area, leading to the increase of internal energy.

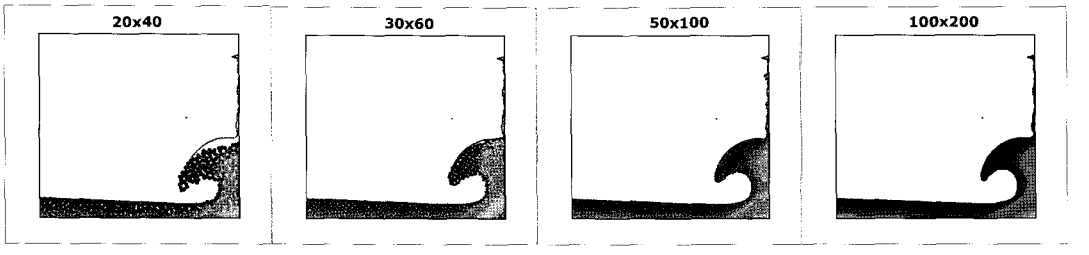


(a) t=1.4 sec

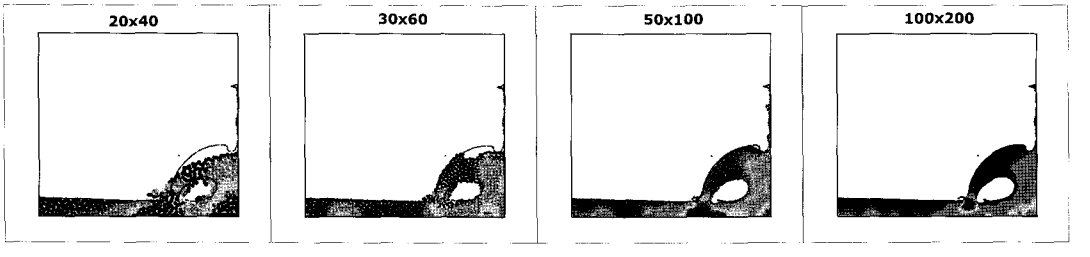


(b) t=1.5 sec

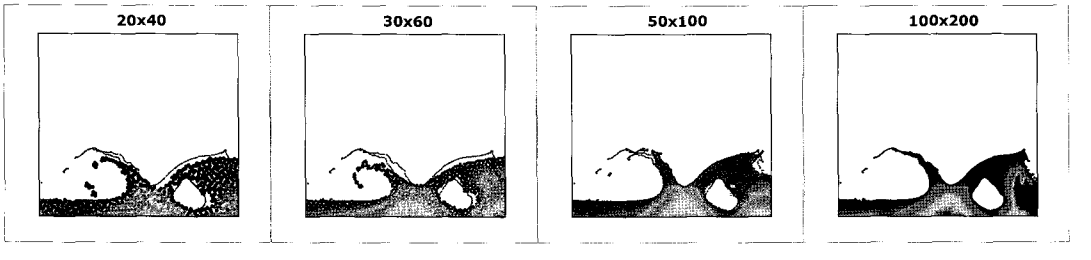


(c) t=1.7 sec

**Figure 8:** Free surface profile (solid line is that of 100 x 200)

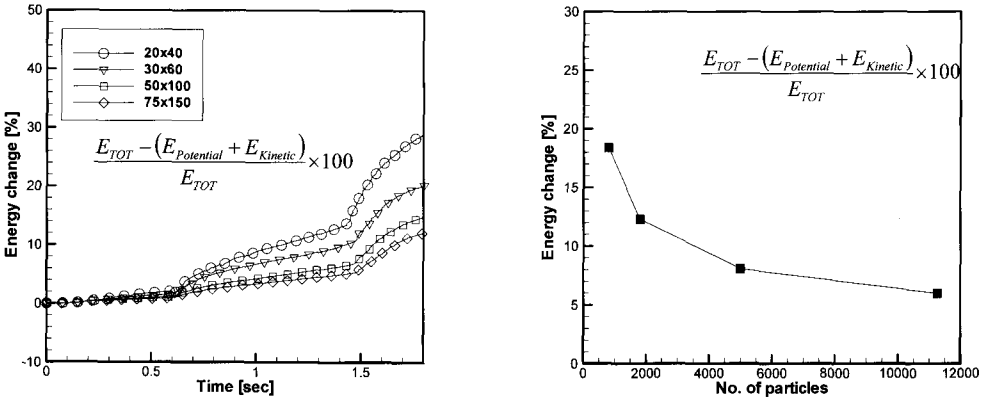


(a) Energy change w.r.t time (b) Energy change w.r.t No. of particles

**Figure 9:** Energy change depending on the No. of particles

Figure 10 shows the time-histories of pressure for the different numbers of particles at the location where an arrow points. As expected, the fluctuation of pressure signal tends to decrease as the number of particles increases. Pressure on the wall is extracted at the specified location by applying the Shepard interpolation.

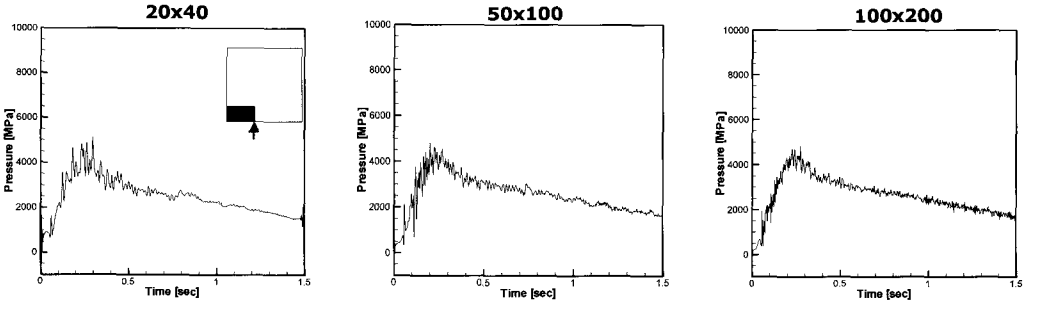


**Figure 10:** Pressure time history

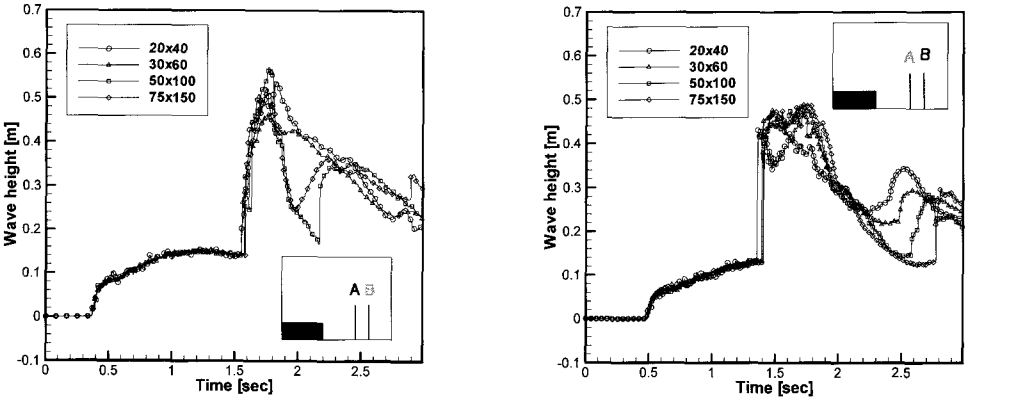


(a) A: 2.2m sway from the left wall (b) B: 2.7m sway from the left wall

**Figure 11:** Wave height evolution (A:2.2m, B:2.7m away from left wall)

Figure 11 shows the evolution of wave height at two locations, A and B, located at 2.233m and 2.725m away from the left vertical wall. What draws attention in this graph is that, before overturning wave comes back to the location A and B, i.e. around 1.5-sec, there is little difference in wave height evolution even though the numbers of particles differ a lot. This means that SPH can capture the primary evolution of free surface even in the case that the number of particles is not sufficient. However, as expected, deviation becomes large as violent free surface develops in the tank. According to the results in Figure 10, it can be said that convergence of SPH solution in a very strict sense is not easy to mention.

## 4.2 Speed of sound

The state equation, Eq. (10), involves the speed of sound in the computation of pressure. The factor $B$ is proportional the square of the speed of sound, taking the following form:

$$B = \frac{\rho_0 c^2}{\gamma} \tag{13}$$

When particles are evenly distributed and stay still at the beginning of analysis, density gradient equals to zero, meaning that pressure gradient and corresponding acceleration are zero as well. When a particle starts to move closer to neighboring particle, the density gradient will increase leading to the increase of pressure gradient. Considering two different materials with two different speeds of sound, the pressure gradient of the material with a higher speed of sound will increase far more than that with a lower speed of sound, leading to bigger repulsive force between particles. Similar situation happens when particles get separated. When this is the case, the density gradient will drop, causing the decrease of pressure gradient and consequently leading to the generation of attraction force. Again, this attraction force will be larger when the speed of sound is larger. Figure 12 schematically illustrates how speed of sound affects particle interaction.

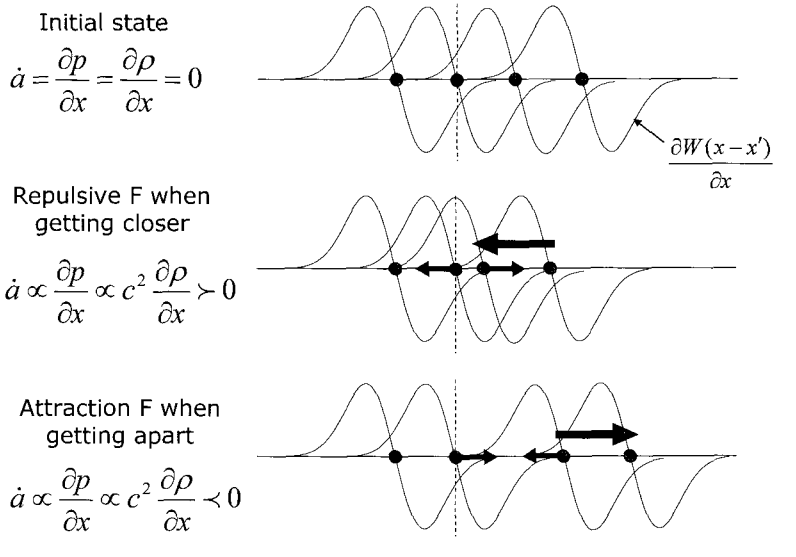


**Figure 12:** Role of speed of sound

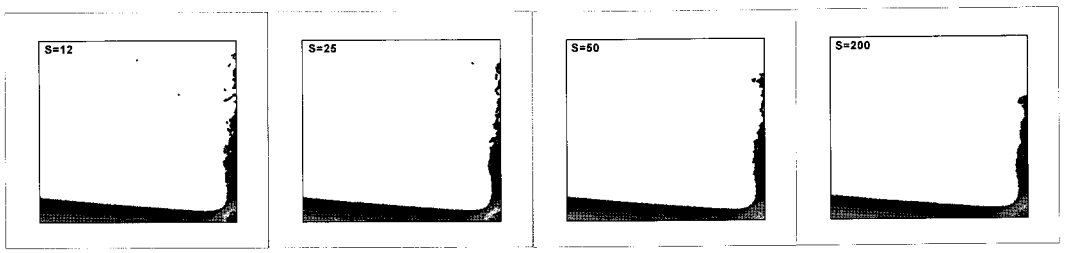


(a) t=1.0 sec

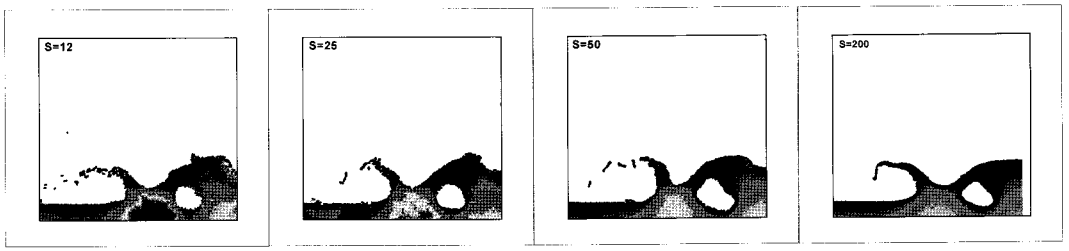


(b) t=1.7 sec

**Figure 13:** Dependency on the speed of sound: from left 12, 25, 50, and 200m/sec, 5,000 particles

Based on the above explanation about the role of the speed of sound in SPH simulation, it can be concluded that particle separation is less likely to happen when the speed of sound get bigger. Figure 13 clearly shows such trend. It can be seen that the number of spattering particles tends to decrease as the speed of sound becomes big. Since actual speed of sound of water is 1500m/sec, which is far bigger than 200m/sec, maximum value in Figure 13, it is less likely to see spattering particles when actual speed of sound is used in the analysis. However, trade-off between simulation accuracy and computational cost always needs to be considered so that actual speed of sound is hard to be used. Therefore, it should be emphasized that the spatter of water particles in SPH simulation does not happen always due to physical reason, but sometimes numerical reason.

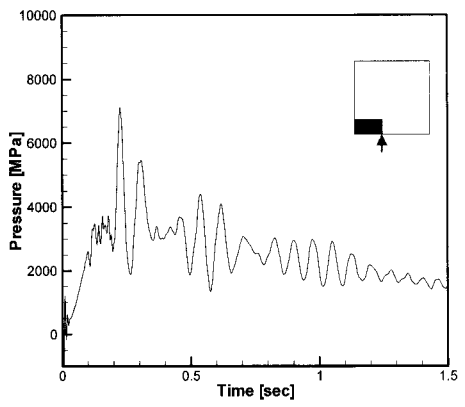


(a) Speed of sound = 12 m/sec

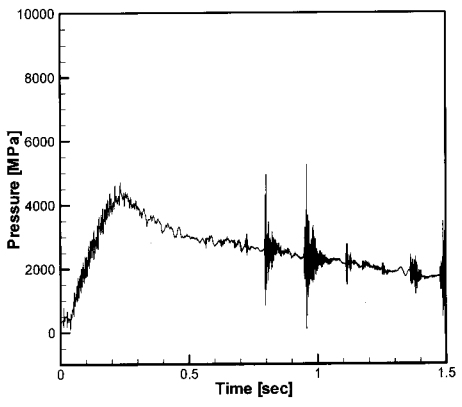


(b) Speed of sound = 200 m/sec

**Figure 14:** Pressure time histories for two speeds of sound

Figure 14 shows the time-history of pressure at a point inside the tank. When the sound speed is extremely low -reasonable value is about 50 m/sec in this analysis, based on the Mach number of 0.1, pressure signal oscillates a lot, like Figure 14(a). This is due to the fact that the speed of sound makes the fluid too compressible, therefore pressure fluctuates in very slow manner. Figure 14(b) shows that oscillatory behavior of pressure decreases significantly, thanks to the extremely weakened compressibility. Pressure waves still travel through fluid, but with much higher speed ending up with very short wave length.

Figure 15 shows density fluctuation with respect to the speed of sound. As was explained, a larger speed of sound makes the stiffer equation of state and cases less density fluctuation. Again, this means that the fluid becomes less and less compressible. Drastic density change occurs around 0.6-sec when the surge front of collapsing dam hits the right vertical wall. The density fluctuation stays below 10% when speed of sound was set to be 50 m/sec, which is roughly 10 times maximum velocity of fluid throughout the analysis. Figure 15(b) shows that maximum density fluctuation converges to zero in monotonic way as the speed of sound increases.

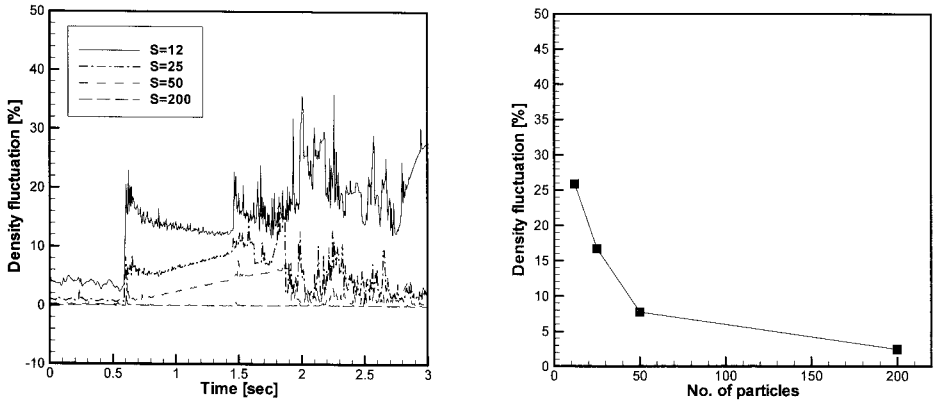


(a) Density fluctuation w.r.t time (b) Density fluctuation w.r.t speed of sound

**Figure 15:** Density fluctuation

## 4.3 Frequency of density re-initialization

In SPH simulation for weakly compressible flow, two state variables are marched in time domain according to the governing partial differential equation. Those variables are density and velocity. The velocity vector is marched following the momentum equation which links acceleration to pressure gradient and external body force. On the other hand, the density field is updated by the continuity equation which connects density time rate to velocity divergence. However, if the continuity equation is used for the evolution of density field, consistency among pre-specified particle mass, density and volume may be lost(Monaghan[14]). This inconsistency can be overcome by so called density re-initialization(Colagrossi[7]). To achieve this, density field is reset after a certain number of time steps by using Eq. (14).

$$\rho_i = \sum_j \rho_j W_{ij} \Delta V_j = \sum_j m_j W_{ij} \tag{14}$$

When Eq. (14) is applied, a special care should be given to avoid particle deficiency problem. Colagrossi[7] suggested to use a moving least square scheme to guarantee the reproducibility of interpolation up to the first order, which the inversion of 3 x 3 matrix is required for every particles. In the present study, however, the Shepard interpolation is used mainly because it reduces computational cost significantly without deteriorating interpolation accuracy considerably. The key in this parametric study is to know how often density re-initialization needs to be done for observing the improvement of solution accuracy. To this end, four different cases were analyzed, from re-initializing density for every time step, through every 5 and 20 time steps, up to infinite, meaning no density re-initialization at all.

Figure 16 clearly demonstrates that benefits are considerable when periodic density re-initialization is applied. Spiky pressure field was smoothed, then the improvement of velocity field can be expected as well. Figure 17 shows dramatic improvement in pressure signal when the frequency of density re-initialization is frequent. It is also shown that the re-initialization conserves energy much better than original SPH formulation because re-initialization process is more or less like spatial filter which reduces high frequency oscillation. In consequence, energy dissipation by artificial viscosity(Colagrossi[7]) can be minimized.

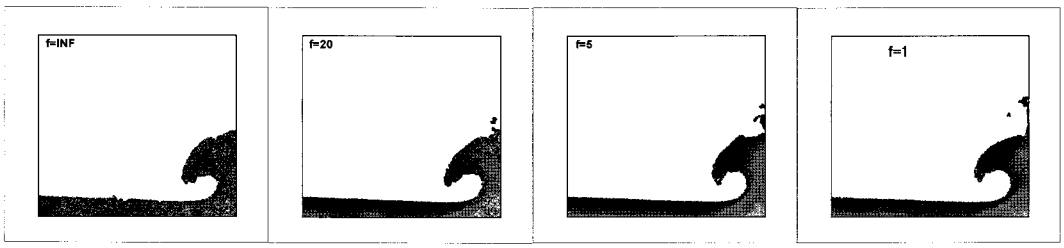


(a) t=1.4 sec

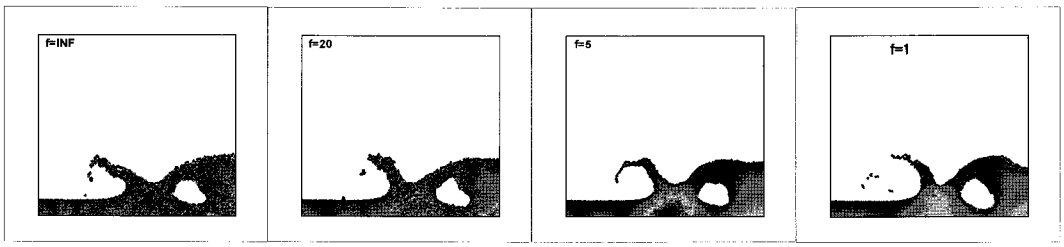


(a) t=1.7 sec

**Figure 16:** Improvement of pressure field due to density re-initialization: from left, no re-initializing, once in 20, 5, and 1 time steps, 5,000 particles

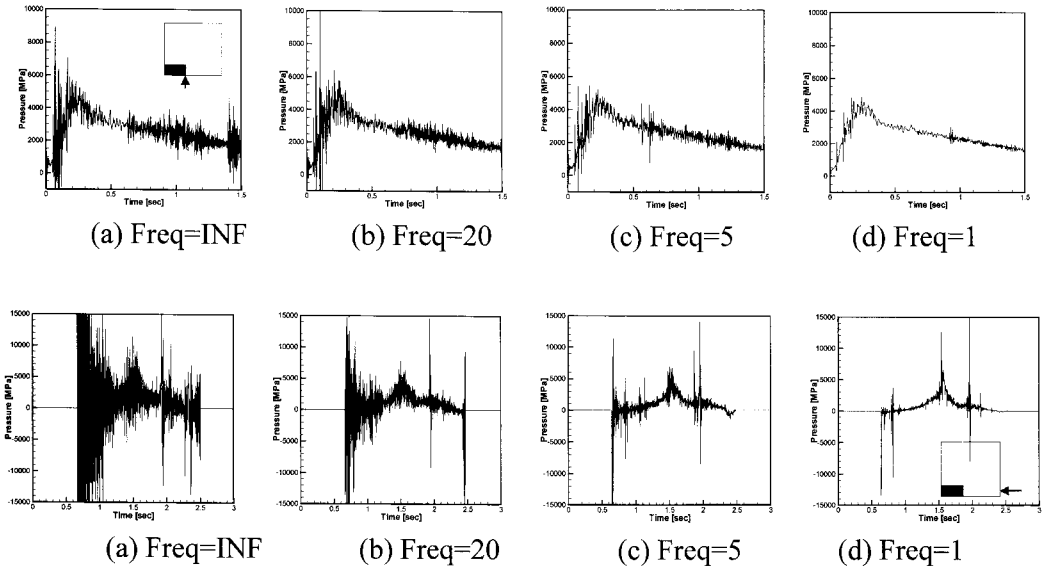


**Figure 17:** Pressure time-histories for different intervals of density re-initialization

## 4.4 Type of smoothing function

Proper choice of smoothing function has utmost importance in SPH simulation. This is because, in meshless methods like SPH, interpolation is made based on the particles which are arbitrarily scattered throughout the whole domain without any connectivity between them. Under this circumstance, smoothing function and its first derivative are the only parameters that determine how particles interact each other. There are some necessary requirements of smoothing function, as follows:

- Partition of unity : $\int W(x-x',h)dx = 1$
- Compact supportness : $W(x-x') = 0,\ |x-x'| > \kappa h$
- Property of Dirac delta function : $\lim_{h\to 0} W(x-x',h) = \delta(x-x')$

A Gaussian function is one of the most popular one among various smoothing functions. Figure 18 shows smoothing function and its first derivative of Gaussian, quadratic and cubic function respectively. Some use a quartic function as shown in Eq.(16). Gaussian, cubic and quadratic have basically same shape in function itself, but its first derivatives are different from each other. The quadratic function is quite different from others since it has sharp peak at center so as to have ever increasing first derivative when approaching zero. This quadratic smoothing function was firstly introduced by Johnson and Beissel[15] who claimed that it is an improvement over cubic spline smoothing function. The first derivative of the quadratic function does not go down to zero when neighboring particle enters within the distance of $2/3h$ where peak of its first derivative appears in case of cubic function, which is intuitively more realistic.

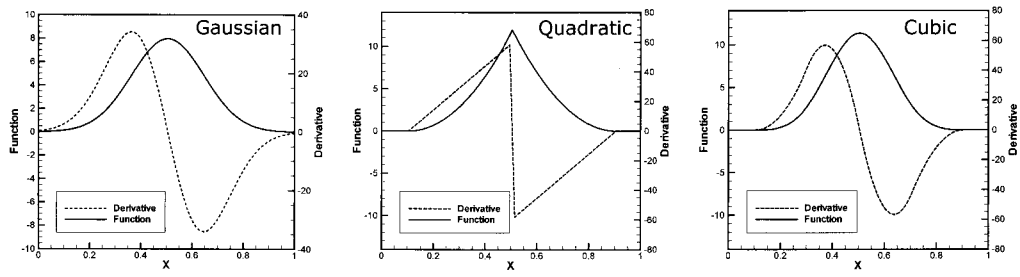


**Figure 18:** Various smoothing function

Eq. (15) to (18) shows Gaussian, quadratic, cubic and quartic smoothing functions.

$$\text{Gaussian: } W(R,h) = \frac{1}{\pi h^2} e^{-R^2} \quad , R = \frac{|x - x'|}{h} \tag{15}$$

$$\text{Quadratic: } W(R,h) = \frac{2}{\pi h^2}\left(\frac{3}{16}R^2 - \frac{3}{4}R + \frac{3}{4}\right) \quad 0 \le R \le 2 \tag{16}$$

$$\text{Cubic: } \begin{aligned} W(R,h) &= \frac{15}{7\pi h^2}\left(\frac{2}{3} - R^2 + \frac{1}{2}R^3\right) && ,0 \le \mathrm{R} < 1 \\ &= \frac{15}{7\pi h^2}\left[\frac{1}{6}(2-R)^3\right] && ,1 \le \mathrm{R} < 2 \\ &= 0 && ,2 \le \mathrm{R} \end{aligned} \tag{17}$$

$$\text{Quartic: } W(R,h) = \frac{15}{7\pi h^2}\left(\frac{2}{3} - \frac{9}{8}R^2 + \frac{19}{24}R^3 - \frac{5}{32}R^4\right) \quad 0 \le \mathrm{R} < 2 \tag{18}$$

Figure 19 shows free surface profiles at t=1.4 sec for different smooth functions. It can be said that differences are relatively minor in the sense that all are quite good in capturing free surface profile, but particles near the tip of plunging wave behave in slightly different way.

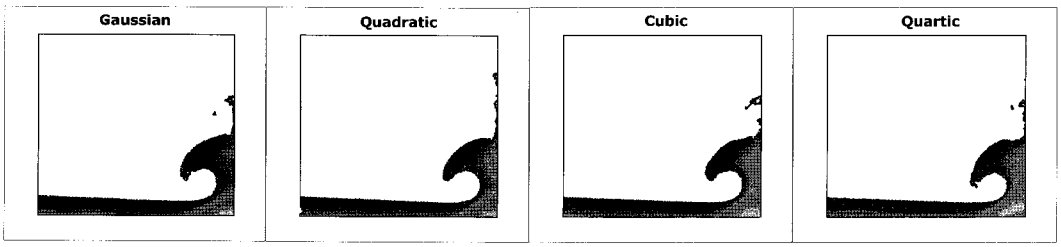


**Figure 19:** Free surface profile (t=1.4sec, 5,000 particles)

Figure 20 shows the detailed comparison of free surface profile between those of the Gaussian and quadratic functions. Both are directly compared with the result with 20,000

particles. According to these results, the quadratic function provides free surface profile smoother than that of the Guassian distribution. In particular, particles near the tip of plunging wave seem to behave more orderly at the moment right before plunging wave hits horizontal free surface. Same situation happens after rebound of plunging wave forming second water splash as shown in Figure 20(b). Though the reason why the quadratic function seems to work better than the Gaussian is not clear at this moment, there are several aspects that the quadratic smoothing function has edge over the Gaussian-type smoothing function. As explained, unlike Gaussian type smoothing function, the first derivative of the quadratic function does not have its peak, whereas it always tends to move down to zero as inter-particle distance becomes very small in case of the Gaussian smoothing. This means that the quadratic function is better in preventing inter-particle penetration since the weight of approaching nearest neighboring particle always increases, which is desirable. Again, this characteristic of the first derivative of the quadratic smoothing function keeps compressive softening from occuring. It can be also pointed out that tensile instability which is inevitable in SPH simulation may be reduced by using quadratic smoothing function(Monaghan[4]).

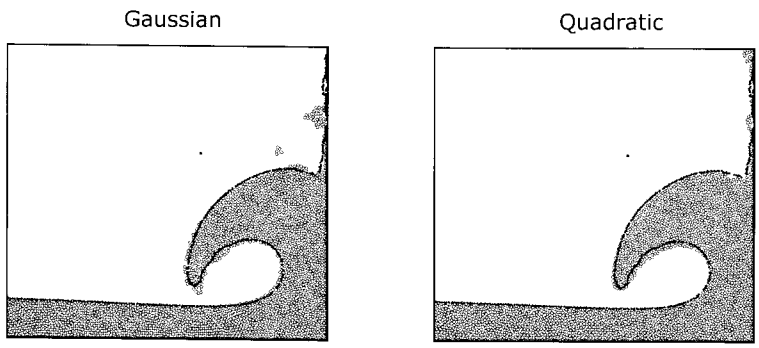


(a) t=1.45 sec

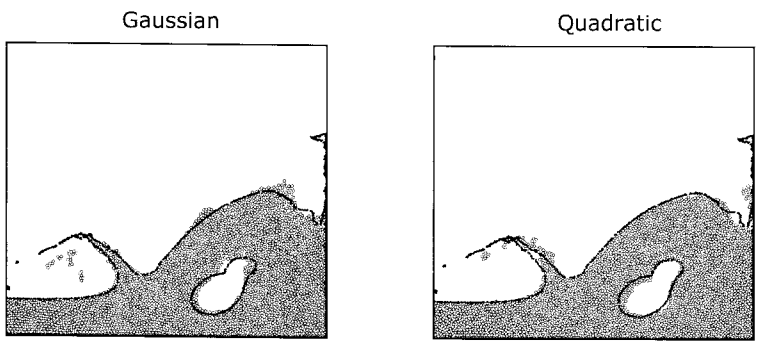


(b) t=1.6 sec

**Figure 20:** Free surface profile (5,000 particles, solid line from 20,000 particles)

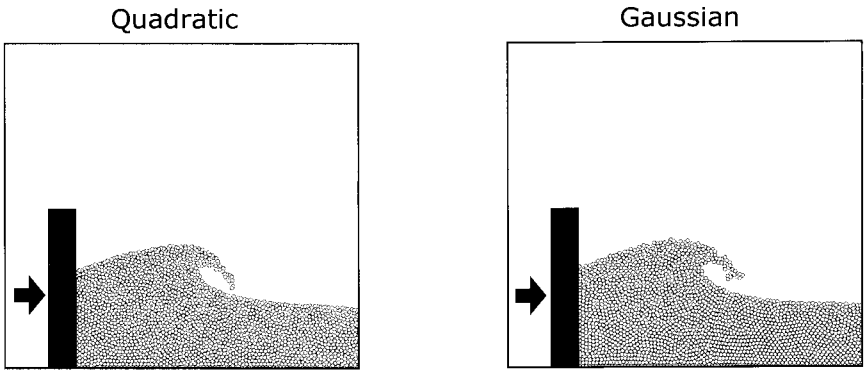


**Figure 21:** Free surface profile of breaking wave

The role of tensile instability as a source of differences between the two smoothing functions may be backed by the fact that tensile stress becomes present only near the free surface where differences is observed noticeably, especially near the tip of plunging wave.

Figure 21 shows the simulation results of wave breaking. Initially calm water was excited by a piston-type wave maker placed at the left end of numerical basin. When excitation frequency becomes high enough with amplitude unchanged, wave tends to break at the very early stage of its propagation. It can be observed that similar situation happens in this wave breaking problem if focus is on the tip of plunging wave. Particles are more orderly distributed when the quadratic smoothing function was used. Again, this is the area where negative pressure becomes present having the chances of tensile instability.

## 4.5 Smoothing length

Smoothing length is the size of smoothing function, $h$, in Eq. (15)~(18), indicating the level of smoothing. For a given number of particles, smoothing will be done in larger area if the smoothing length becomes larger, meaning that field will be more and more smoothed but spatial resolution becomes less and less accurate. In this sense, the smoothing length plays a role similar to grid resolution in grid-based numerical methods. In the present case, the level of smoothing is strongly linked to both smoothing length and the number of particle. Therefore, it may be desirable to have more particles in computational domain with smaller smoothing length, keeping a enough number of neighboring particles inside a support domain.

Figure 22 shows free surface profiles for two different smoothing lengths, 0.7 and 0.9 times initial particle space, $\Delta s$. The Gaussian smoothing function was used in this simulation. Figure 22(a) shows that pressure field is far smoother when the larger smoothing length was used. When free surface becomes more violent as in Figure 22(b), free surface profile with smaller smoothing length becomes very poor compared to the case of the larger smoothing length.

Figure 23 shows pressure time history at two different locations: one on the tank bottom and the other on the right vertical wall. It clearly demonstrates that the number of neighboring particles getting involved in the SPH smoothing process is a key to achieve sufficient accuracy. The number of neighboring particles is between 13~17 in case of

0.7Δs, while it is between 20~25 in case of 0.9Δs. 0.85Δs ~0.9Δs seems to be reasonable choice for the Gaussian smoothing function without the loss of local behavior.

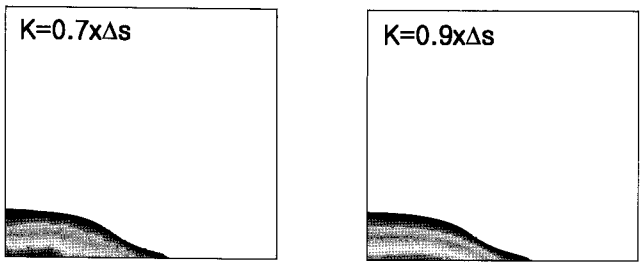


(a) t=0.3 sec

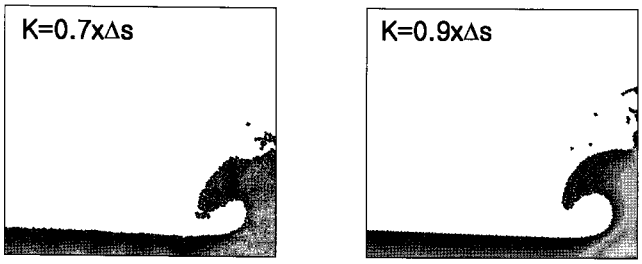


(b) t=1.4 sec

**Figure 22:** Free surface profiles for different smoothing lengths (5,000 particles)

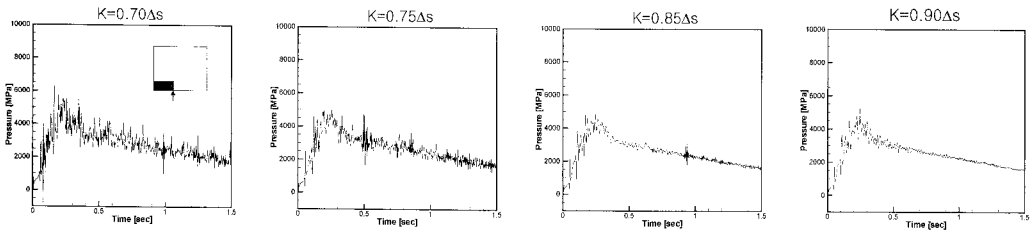


(a) On the bottom

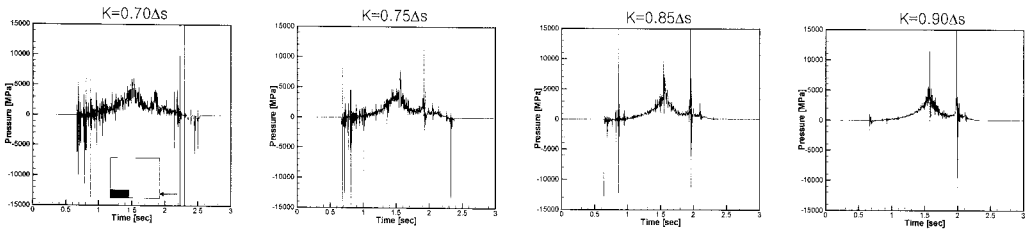


(b) On the right vertical wall

**Figure 23:** Pressure time history w.r.t smoothing length

The smoothing length could be of course larger than 0.9Δs leading to smoother field. However, as mentioned before, it will deteriorate spatial resolution. Moreover, increasing

the number of neighboring particles increases the number of total pair of interacting particles, ending up with longer analysis time. Many literatures recommend about or slightly more than 20 for the optimal number of neighboring particles. Another problem that may be met when the number of neighboring particle increases is that particles near the solid wall tend to penetrate into the wall.

As to SPH interpolation itself, the convergence of interpolation error can be expressed as follows(Mas-Gallic and Raviart[16]):

$$Err = h^2 + h^{-n}\left(\frac{\Delta x}{h}\right)^2 \tag{19}$$

where $n$ is the order of derivative. Eq.(19) indicates that interpolation error tends to decrease when smoothing length gets smaller and the ratio of particle space to smoothing length becomes small. Regarding the second term, in order to achieve the convergence of SPH interpolation, it should be kept that the particle space decreases faster than the decrease of the smoothing length. If the ratio of the particle space to the smoothing length is kept constant when refining, interpolation error will never converge to zero(Colagrossi[7]).

## 4.6 Wall pressure(pressure extraction method)

Three different methods are considered to compute hydrodynamic pressure acting on the solid wall. SPH interpolation scheme, direct calculation from nearest particle and pressure sensor approach are those.

Method I : In this scheme, pressure on the wall is calculated based on the original SPH interpolation formula. In order to overcome boundary deficiency problem, which is inevitable near the solid wall, Shepard interpolation was used as Eqn(20).

$$P_M = \frac{\sum_j P(\vec{r}_j) W(\vec{r}_i - \vec{r}_j, h)\frac{m_j}{\rho_j}}{\sum_j W(\vec{r}_i - \vec{r}_j, h)\frac{m_j}{\rho_j}} \tag{20}$$

Method II : Pressure on the wall is calculated based on the pressure value of the nearest particle. Instead of directly using the value, correction was made to compensate hydrostatic pressure which is caused by the difference of vertical position between the pressure point and its nearest particle.

$$P_M = P_{closest} - \rho_i g(y_{closest} - y_i) \tag{21}$$

Method III : In this scheme, pressure is averaged over the size of pseudo pressure sensor. Particles near solid wall within the distance of 1.5h and the width $S_{sensor}$, which is the width of pseudo pressure sensor, are searched first. Then the pressure of each sampled particle(i) is projected(i') to the wall. These particles are sorted sequentially in tangential direction, following the curvilinear abscissa **q**, which is parallel to the arbitrarily curved wall. Finally, the pressure at the position of interest is obtained following the formula.

$$P_M = \frac{\int_{S_{sensor}} PdS}{\int_{S_{sensor}} dS} \approx \frac{\sum_{i'} P_{i'} dS_{i'}}{\sum_{i'} dS_{i'}} \tag{22}$$

where $dS_{i'} = \frac{q_{i'+1} - q_{i'-1}}{2}$, $P_{i'} = P_i - \rho_i g(y_{i'} - y_i)$

The detailed procedure of Method III can be found in Oger et.al.[17].

Figure 24 shows pressure time history which was obtained based on the aboved mentioned procedures applied to the 2D sloshing problem of Figure 7. Method I, based on the origianl SPH interpolation, shows minimal pressure fluctuation among the cases. Overall trends are pretty similar between different schemes, but different spikiness level led to different pressure value at its peak and valley.

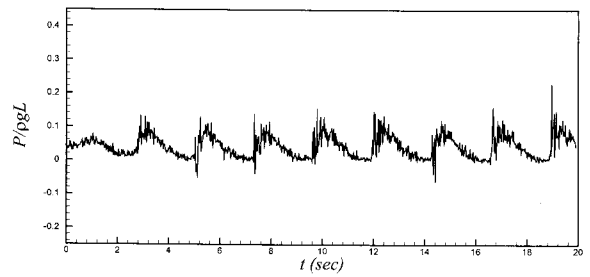


(a) Method I

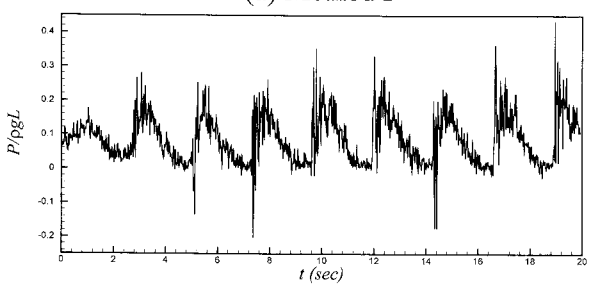


(b) Method II

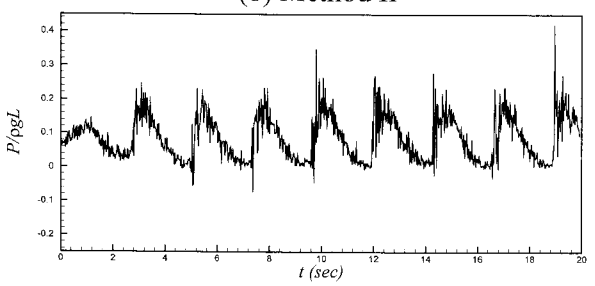


(c) Method III

**Figure 24:** Comparison of local pressure time history (y=0.0175 of left vertical wall, w=2.7, h/b=0.08)

## 5 Conclusions

In the present study, comprehensive numerical tests have been done to gather information about what the aftermath of parameter change is in SPH simulation as well as how solution accuracy can be improved without touching the fundamentals of scheme itself. The gathered information can be summarized as follows.

- Similar to other discretization-based numerical schemes, SPH also shows converging property in its nature when the number of particle used in the analysis increases, though quantitative evaluation is not easy to perform. In order to increase convergence rate, the ratio of initial particle space to smoothing length should decrease while increasing number of particle. Good news is that energy loss -actually it is not loss- to internal energy plus to viscous dissipation tends to decrease in monotonic way when number of particle increases. Also, spiky behavior of pressure time history tends to decrease with the increase of particle number.
- The speed of sound is one of the most important analysis parameters in SPH simulation. Generally, to simulate incompressible fluid flow by weakly compressible approach, the speed of sound is set to be 10 times of the expected maximum velocity. The speed of sound plays a very important role in particle spattering, which resembles real physical phenomenon. However, in some sense, this particle spattering is induced by imaginarily low sound speed, which is the consequence of trade-off between solution accuracy and computational efficiency. Nevertheless, such spatter of particle is not completely far from real physical phenomena since the splash occurs in actual physical problems.
- It turned out that the use of periodic density re-initialization provides huge improvement to the results of SPH simulation. The density re-initialization process works pretty well in removing the spikiness of pressure-time signal as well as smoothing pressure field itself. In the present case, the more frequent re-initialization is carried out, the better results it produces.
- The type of smoothing function basically has minor influence to SPH simulation results. The unique characteristics of quadratic smoothing function, ever increasing first derivative when particles get closer, seems to generate better results especially near the tip of plunging wave, where tensile stress is always present. If discussion is confined only to the interpolation capability of smoothing function, it can be said that Gaussian or cubic is better than quadratic especially when particles are disorderly distributed. However, this gap can be overcome by using normalization of smoothing function, like Shepard interpolation.
- Smoothing length needs to be large enough to include a sufficient number of neighboring particles for accurate interpolation. At the same time, it shouldn't be too large in order not to smooth out all the details of local behavior. In case of Gaussian smoothing function, when smoothing length becomes larger than 0.9 times initial particle space, problems occurs near the solid wall such as particle penetration into the wall.
- Three different schemes used to extract wall pressure were examined to see how accurately each scheme captures local wall pressure. It is not easy to make clear conclusion about which method is best due to the spikiness in pressure time history. Further investigation is required to find out accurate pressure extraction scheme.

## References

Colagrossi, A. 2005. A Meshless Lagrangian Method for Free-Surface and Interface Flows with Fragmentation. PhD Thesis University of Roma.

Colagrossi, A. and M. Landrini. 2003. Numerical Simulation of Interfacial Flows by Smoothed Particle Hydrodynamics. Journal of Computational Physics, **191**, 448-475.

Dalymple, R.A. and B.D. Rogers. 2006. Numerical Modeling of Water Waves with the SPH Method. Coastal Engineering, **53**, 141-147.

Dilts, G. 1999. Moving-least-squares-particle Hydrodynamics – I. Consistency and Stability. International Journal for Numerical Methods in Engineering, **48**, 1115-1155.

Dilts, G. 2000. Moving-least-squares-particle Hydrodynamics – II. Conservation and Boundaries. International Journal for Numerical Methods in Engineering, **48**, 1504-1524.

Johnson, G.R. and S.R. Beissel. 1996. Normalized Smoothing Functions for SPH Impact Computations. International Journal for Numerical Methods in Engineering, **39**, 2725-2741.

Liu, G.R. and M.B. Liu. 2003. Smoothed Particle Hydrodynamics -A Meshfree Particle Method-. World Scientific Publishing Co. Ltd.

Liu, M.B., G.R. Liu. and K.Y. Lam. 2003. Constructing Smoothing Functions in Smoothed Particle Hydrodynamics with Applications. Journal of Computational and Applied Mathematics, **155**, 263-284.

Liu, M.B. and G.R. Liu. 2006. Restoring Particle Consistency in Smoothed Particle Hydrodynamics. Applied Numerical Mathematics, **56**, 19-36.

Li, S. and W.K. Liu. 2004. Meshfree Particle Methods. Springer.

Li, S. and W.K. Liu. 2002. Meshfree and Particle Methods and Their Applications. Appl. Mech. Rev., **55**, 1-34.

Libersky, L.D. and A.G. Petschek. 1990. Smooth Particle Hydrodynamics with Strength of Materials. Advances in the Free Lagrangian Method, Lecture Notes in Physics, **395**, 248-257.

Mas-Gallic, S. and P. Raviart. 1987. A Particle Method for First-order Symmetric Systems. Numer. Math., **51**, 323-352.

Monaghan, J.J. 1992. Smoothed Particle Hydrodynamics. Annu. Rev. Astron. Astrophys., 543-574.

Monaghan, J.J. 1983. Shock Simulation by the Particle Method SPH. Journal of Computational Physics, **52**, 374-389.

Monaghan, J.J. 1994. Simulating free surface flow with SPH. Journal of Computational Physics, **110**, 399-406.

Monaghan, J.J. 2000. SPH without a Tensile Instability. Journal of Computational Physics, **159**, 290-311.

Monaghan, J.J. and A. Kos. 1999. Solitary Waves on a Cretan Beach. Journal of Waterway, Port, Coastal and Ocean Engineering, 145-154.

Nam, B.W. and Y. Kim. 2006. Simulation of Two-Dimensional Sloshing Flows by SPH Method. Proceedings of ISOPE-2006, San Francisco USA.

Oger, G., M. Doring, B. Alessandrini and P. Ferrant. 2005. Two-dimensional SPH Simulations of Wedge Water Entries. Journal of Computational Physics, **213**, 803-822.

Riffert, H, H. Herold, O. Flebbe and H. Ruder. 1995. Numerical Aspects of the Smoothed Particle Hydrodynamics Method for Simulating Accretion Disks. Computer Physics Communications, **89**, 1-16.

Shepard, D. 1968. A Two-Dimensional Interpolation Function for Irregularly-Spaced Data. Proceedings of the 23rd National Conference, ACM, 517-523.

Souto-Iglesias, L., L. Perez-Rojas and R. Zamora-Rodriguez. 2004. Simulation of Anti-roll Tanks and Sloshing type Problems with Smoothed Particle Hydrodynamics. Ocean Engineering, **31**, 1169-1192.

Swegel, J.W., D.L. Hicks and S.W. Attaway. 1995. Smoothed Particle Hydrodynamics Stability Analysis. Journal of Computational Physics, **116**, 123-134.

Van Daalen, E.F.G. 1999. Two–dimensional free surface anti-roll tank simulations with a volume of fluid based Navier-Stokes solver. Report No. 15306-1-OE, MARIN.